Original Article

MOLECULAR METABOLISM

Hepatocyte-specific O-GlcNAc transferase downregulation ameliorates nonalcoholic steatohepatitis by improving mitochondrial function

Maria J. Gonzalez-Rellan [1,2,*,14], Tamara Parracho [1,14], Violeta Heras [1], Amaia Rodriguez [2,3], Marcos F. Fondevila [1,2], Eva Novoa [1,2], Natalia Lima [1], Marta Varela-Rey [4], Ana Senra [1], Maria D.P. Chantada-Vazquez [5], Cristina Ameneiro [6], Ganeko Bernardo [7], David Fernandez-Ramos [7], Fernando Lopitz-Otsoa [7], Jon Bilbao [7], Diana Guallar [6], Miguel Fidalgo [1], Susana Bravo [5], Carlos Dieguez [1,2], Maria L. Martinez-Chantar [7], Oscar Millet [8,13], Jose M. Mato [8,13], Markus Schwaninger [9], Vincent Prevot [10], Javier Crespo [11], Gema Frühbeck [2,3], Paula Iruzubieta [11], Ruben Nogueiras [1,2,12,]**

ABSTRACT

Objective: *O*-GlcNAcylation is a post-translational modification that directly couples the processes of nutrient sensing, metabolism, and signal transduction, affecting protein function and localization, since the *O*-linked N-acetylglucosamine moiety comes directly from the metabolism of glucose, lipids, and amino acids. The addition and removal of *O*-GlcNAc of target proteins are mediated by two highly conserved enzymes: *O*-linked N-acetylglucosamine (*O*-GlcNAc) transferase (OGT) and *O*-GlcNAcase (OGA), respectively. Deregulation of *O*-GlcNAcylation has been reported to be associated with various human diseases such as cancer, diabetes, and cardiovascular diseases. The contribution of deregulated *O*-GlcNAcylation to the progression and pathogenesis of NAFLD remains intriguing, and a better understanding of its roles in this pathophysiological context is required to uncover novel avenues for therapeutic intervention. By using a translational approach, our aim is to describe the role of OGT and *O*-GlcNAcylation in the pathogenesis of NAFLD.

Methods: We used primary mouse hepatocytes, human hepatic cell lines and *in vivo* mouse models of steatohepatitis to manipulate *O*-GlcNAc transferase (OGT). We also studied OGT and *O*-GlcNAcylation in liver samples from different cohorts of people with NAFLD.

Results: *O*-GlcNAcylation was upregulated in the liver of people and animal models with steatohepatitis. Downregulation of OGT in NAFLD-hepatocytes improved diet-induced liver injury in both *in vivo* and *in vitro* models. Proteomics studies revealed that mitochondrial proteins were hyper-*O*-GlcNAcylated in the liver of mice with steatohepatitis. Inhibition of OGT is able to restore mitochondrial oxidation and decrease hepatic lipid content in *in vitro* and *in vivo* models of NAFLD.

Conclusions: These results demonstrate that deregulated hyper-*O*-GlcNAcylation favors NAFLD progression by reducing mitochondrial oxidation and promoting hepatic lipid accumulation.

Keywords *O*-GlcNAcylation; Mitochondrial dysfunction; NAFLD

[1]Department of Physiology, CIMUS, University of Santiago de Compostela, Spain [2]CIBER Fisiopatologia de la Obesidad y Nutrición (CIBERobn), Spain [3]Metabolic Research Laboratory, Clínica Universidad de Navarra and IdiSNA, Pamplona, Spain [4]Gene Regulatory Control in Disease, CIMUS, University of Santiago de Compostela, Santiago de Compostela, Spain [5]Proteomic Unit, Health Research Institute of Santiago de Compostela (IDIS), Santiago de Compostela, 15705, A Coruña, Spain [6]Department of Biochemistry and Molecular Biology, CIMUS, University of Santiago de Compostela-Instituto de Investigación Sanitaria, Santiago de Compostela, Spain [7]CIC bioGUNE, Centro de Investigación Biomédica en Red de Enfermedades Hepáticas y Digestivas (Ciberehd), Technology Park of Bizkaia, Derio, 48160, Bizkaia, Spain [8]Liver Disease Laboratory, Center for Cooperative Research in Biosciences (CIC bioGUNE), Basque Research and Technology Alliance (BRTA), Bizkaia Technology Park, Building 801A, 48160, Derio, Spain [9]University of Lübeck, Institute for Experimental and Clinical Pharmacology and Toxicology, Lübeck, Germany [10]Univ. Lille, Inserm, CHU Lille, Laboratory of Development and Plasticity of the Neuroendocrine Brain, Lille Neuroscience & Cognition, UMR-S 1172, European Genomic Institute for Diabetes (EGID), F-59000, Lille, France [11]Gastroenterology and Hepatology Department, Marqués de Valdecilla University Hospital, Clinical and Translational Digestive Research Group, IDIVAL, Santander, Spain [12]Galicia Agency of Innovation (GAIN), Xunta de Galicia, Santiago de Compostela, Spain [13]Centro de Investigación Biomédica en Red de Enfermedades Hepáticas y Digestivas (Ciberehd) Technology, Spain

[14] Maria J. Gonzalez-Rellan and Tamara Parracho contributed equally to this work.

*Corresponding author. Department of Physiology, CIMUS, University of Santiago de Compostela, Spain. E-mail: chusa.gzlz.rellan@gmail.com (M.J. Gonzalez-Rellan).

**Corresponding author. Department of Physiology, CIMUS, University of Santiago de Compostela, Spain. E-mail: ruben.nogueiras@usc.es (R. Nogueiras).

Received May 24, 2023 • Revision received July 7, 2023 • Accepted July 9, 2023 • Available online 13 July 2023

https://doi.org/10.1016/j.molmet.2023.101776

1. INTRODUCTION

Non-alcoholic fatty liver disease (NAFLD) is currently the leading cause of chronic liver disease, affecting 25% of the global population [1]. The hallmark of NAFLD is an accumulation of lipids in the liver resulting from deranged lipid and/or glucose metabolism. Consequently, NAFLD is strongly associated with obesity, insulin resistance/diabetes mellitus and dyslipidemia. About 12%–14% of people with NAFLD develop a more aggressive form, known as non-alcoholic steatohepatitis (NASH), which can progress to advanced liver fibrosis, cirrhosis or liver cancer [2,3]. In fact, type 2 diabetes (T2D) is one of the strongest risk factors for the progression of NAFLD, reflecting a close link of progress to the underlying pathophysiological mechanisms [4,5].

Multiple molecular dysfunctions have been associated to insulin resistance, including the well-described *O*-GlcNAcylation modification of proteins in the insulin signaling pathway, which results in insulin resistance [6]. *O*-GlcNAcylation is a posttranslational modification (PTM) that acts as a nutrient sensor and cell-stress mediator [7–9]. It consists of the transfer of a single *N*-acetylglucosamine from UDP-GlcNAc to a serine or threonine residue in a cytoplasmic or nuclear protein, resulting in its modification with a beta-linked *N*-acetylglucosamine (*O*-GlcNAc) [10]. This modification depends on only two enzymes: *O*-GlcNAc transferase (OGT), which catalyzes the transfer of *O*-GlcNAc, and *O*-GlcNAcase (OGA), which removes *O*-GlcNAc [11]. As a PTM, *O*-GlcNAcylation enables cells to respond promptly to internal and external cues by directly and dynamically controlling protein via modulation of their function, expression, localization and stability, among others [11,12].

Maintaining homeostasis of *O*-GlcNAcylation is crucial for the normal function of multiple cellular processes, which range from transcription and translation to signal transduction and metabolism [13]. However, chronic cell stress and nutrient overload can induce the deregulation of *O*-GlcNAcylation, resulting in hyper–*O*-GlcNAcylation of substrate proteins as well as in *O*-GlcNAcylation of distinct proteins that are poor acceptors under physiological conditions [14]. This hinders proper cell functioning and generates a vicious cycle that aggravates cell and tissue conditions [14]. In fact, dysregulation of *O*-GlcNAcylation has been implicated in several complications of chronic liver disease. For instance, *O*-GlcNAcylated proteins have been found to be upregulated in brain samples from patients with liver cirrhosis and hepatic encephalopathy [15] and in tumor tissues from patients with hepatocellular carcinoma (HCC) [16] or NAFLD-induced HCC [17,18]. In the latter case, OGT plays an oncogenic role, generating palmitic acid and reactive oxygen species [17]. However, despite the strong association between NASH and insulin resistance and HCC, the potential role of *O*-GlcNAcylation in the pathogenesis and progression of NAFLD remains unclear.

Here, we evaluated the potential role of *O*-GlcNAcylation in NAFLD progression and the mechanisms underlying this hepatic condition. We identified that hyper-*O*-GlcNAcylation was induced in patients with fibrosis as well as in animal models for fibrosis. Specific OGT downregulation in hepatocytes improved liver damage in mice fed a methionine and choline-deficient (MCD) diet or a choline-deficient plus high fat diet (CD-HFD). Using primary hepatocytes, we corroborated that both pharmacological and genetic inhibition of OGT reduced hepatic lipid content. Based on unbiased proteomics analyses of *O*-GlcNAcylated proteins in the liver of mice with NASH, we identified that mitochondrial proteins were over-represented. Furthermore, downregulation of OGT restored mitochondrial function in hepatocytes incubated with oleic acid (OA) or in MCD medium, while induction of *O*-GlcNAcylation markedly reduced mitochondrial respiration. These results highlight the important role of OGT-induced hyper-*O*-GlcNAcylation in the development of NASH, namely, of inducing mitochondrial dysfunction.

2. PATIENTS AND METHODS

2.1. Animals and diets

Mouse experiments were conducted to the standard protocols approved by the Animal Ethics Committee at the University of Santiago de Compostela (code: 15010/17/007), and mice received the highest levels of human care. C57BL/6J (8-week-old male) mice were housed in rooms under constant temperature (22 °C), a 12:12 h light/dark cycle and with *ad libitum* access to standard diet (STD) (U8200G10R, SAFE), CD-HFD (D05010402; 45 kcal% fat, Research Diets), or a MCD diet (A02082002BR, Research Diets) used during specified times and experiments [19].

2.2. Cohort of patients with NASH for western blot analysis

Liver biopsies were obtained intra-operatively from patients with severe obesity undergoing bariatric surgery ($n = 18$) at the Clínica Universidad de Navarra (Spain). Obesity was defined as a BMI $\geq$ 30 kg/m^2 and body fat percentage as (BF) $\geq$35%. BMI was calculated as weight in kilograms divided by the square of height in meters, and BF was estimated by air-displacement plethysmography (Bod-Pod®, Life Measurements, Concord, CA, USA). Inclusion criteria encompassed a complete diagnostic work-up including physical examination, laboratory investigation, ultrasound echography, and liver biopsy, consistent with the diagnosis of NASH according to the criteria of Kleiner and Brunt by an expert pathologist masked to all results of the assays [20]. Features of steatosis, lobular inflammation, and hepatocyte ballooning were combined to obtain a NAFLD activity score (NAS) (0–8). Exclusion criteria were: a) daily alcohol intake $\geq$20 g for women and $\geq$30 g for men; b) evidence of hepatitis B virus surface antigen or hepatitis C virus antibodies in the absence of a history of vaccination; c) use of drugs causing NAFLD (i.e. amiodarone, valproate, tamoxifen, methotrexate, corticosteroids or anti-retrovirals); and d) presence of other specific liver diseases, such as autoimmune liver disease, haemochromatosis, Wilson's disease, or α-1-antitrypsin deficiency. All reported investigations were carried out in accordance with the principles of the Declaration of Helsinki, as revised in 2013, and approved by the Hospital's Ethical Committee responsible for research (protocol 2017.104). Written informed consent was obtained from all the participants.

2.3. Cohort of patients with NASH for immunostaining analysis

The study population included 13 biopsy-proven NAFLD patients who underwent a liver biopsy with a diagnostic purpose at the Marqués de Valdecilla University Hospital (Santander, Spain). Liver samples with histologically normal condition obtained from 3 subjects during programmed bariatric surgery were used as healthy controls. Inclusion criteria for NAFLD patients were based on an alcohol intake lesser than 20 g/day, the presence of biopsy-proven steatosis with/without necroinflammation and/or fibrosis, and no evidence of hepatitis B and/or C virus infection as well as human immunodeficiency virus (HIV) infection or other causes of liver disease. The characteristics of the NAFLD patients are described in Tables S1 and S2. Hepatic histopathological analysis was performed according to the scoring system of Kleiner et al. [20]. Minimal criteria for NASH included the combined presence of grade 1 steatosis, hepatocellular ballooning, and lobular inflammation with or without fibrosis. This study was performed in agreement with the Declaration of Helsinki and with local and national laws.

The Human Ethics Committees of Valdecilla Hospital approved the study procedures, and written informed consent was obtained from all patients before inclusion in the study.

2.4. Generation of lentiviral particles against OGT

The specific shRNA sequences for knockdown of OGT or scramble shRNA (also targeting Luciferase) were designed using GPP Web Portal Tool (available at https://portals.broadinstitute.org/gpp/public/). The oligos targeting the transcripts of interest were synthesized and subcloned into pLKO.1 puro green fluorescent protein (GFP) vectors (Addgene) as previously described [21]. Briefly, HEK293T cells were maintained in high-glucose DMEM supplemented with 10% FBS (Gibco), 2 mM L-glutamine, and 1% penicillin and streptomycin and plated at a density of 8×10^6 cells per 150 mm dish to be transfected 24 h later with PEI (Polyethylenimine; Sigma–Aldrich, 408727) and 20 μg of pLKO.shRNAs plasmids along with 10 μg of psPAX2 and pMD2.G packaging mix. 24 h later the medium was changed, and virus-containing supernatants were collected 48 h and 72 h post-transfection. Lentiviral particles were concentrated using centrifugal filter units with 0.22 μm pore size (Amicon, UFC903024). The target sequences of the shRNAs used in this study were: shLuciferase: 5′-CCTAAGGTTAAGTCGCCCTCG-3′, shOgt#1: 5′-CCCATTTCTTTCAGCA-GAAAT-3′, and shOgt#2: 5′-GCTCTTAATATGCCCGTTATT-3′.

2.5. Cre activity-specific adeno associated viruses (AAV-FLEX viruses) to downregulate OGT

The AAV-FLEX-shOGT was used in AlfpCre mice to downregulate OGT specifically in the hepatocytes and was purchased from VectorBuilder (#VB210206-1185htu). This AAV FLEX conditional Cre-On gene expression vector is designed to achieve Cre-mediated conditional gene expression in mammalian cells. Expression of the gene of interest is initially silent (in our case the shOGT), however it is permanently activated by co-expression of Cre recombinase, specifically present in the hepatocytes of our AlfpCre mice.

2.6. Tail vein injections for *in vivo* lentiviral and adenoviral gene delivery

Mice were held in a specific restrainer for intravenous injections, Tailveiner (TV-150, Bioseb). The injections into the tail veins were carried out using a 27G × 3/8″ (0.40 mm × 10 mm) syringe. Mice were administered with 100 μl of lentiviral OGT shRNA (1×10^9 TU/ml) or control shRNA (1×10^9 TU/ml), 100 μl of AAV-FLEX-shOGT (1×10^{10} TU/ml) or AAV-FLEX-GFP (1×10^{10} TU/ml) diluted in saline. In the study using mice fed at CD-HFD diet for 12 weeks, the viruses were injected 4 weeks before the sacrifice. In the study using mice fed at MCD diet for 4 weeks, the viruses were injected during the 1st week. Animals were killed by decapitation. Tissues were immediately frozen in dry ice and kept at −80 °C until their analysis.

2.7. Histological procedures

Fresh liver samples were fixed in 4% formaldehyde for 24 h, dehydrated using alcohol 70%, followed to alcohol 80% and 90%, and then embedded in paraffin. Sections of 4 μm were cut with a microtome and stained using a standard Hematoxylin and Eosin alcoholic procedure according to the manufacturer's instructions (BioOptica). After successive rinse with distilled water, sections were dried at 37 °C for 30 min and mounted with permanent (non-alcohol, non-xylene based) mounting media. For Sirius Red staining, liver samples fixated in paraffin were dewaxed, hydrated and stained in Sirius Red staining for one hour. Sections were washed with distilled water, dehydrated in three changes of 100% ethanol and cleared in xylene and mounted in a resinous medium. For Oil Red O staining, frozen liver samples were cut in 8 μm sections with a cryostat and stained in filtered Oil Red O for 10 min. After being washed in distilled water, sections were counterstained with Mayer's hematoxylin for 3 min and mounted in aqueous mounting (glycerin jelly). For Ki67 immunohistochemistry staining, samples fixated in paraffin were dewaxed, hydrated, pre-treated in PTLink TE buffer pH 9 and blocked with 3% peroxidase for 10 min. Next, sections were incubated with the primary antibody (dakoM7248, DAKO) at a concentration of 1:500 overnight and at 4 °C, followed by an incubation with the secondary antibody (EnVision, DAKO) for 30 min at room temperature. After that, DAB developer was used for 1 min and sections were counterstained with Mayer's hematoxylin for 10 min, dehydrated and mounted. For cleaved caspase 3 staining, sections were incubated with a specific primary antibody (#9661, Cell Signaling). In all the histological staining, we used up to 4 representative microphotographs of each animal, which were taken at 20× or 40× with a BX51 microscope equipped with a DP70 digital camera (Olympus). Lipids in Oil Red O-stained sections, collagen depositions in Sirius Red-stained sections and collagen I were quantified using ImageJ software (National Institutes of Health and the Laboratory for Optical and Computational Instrumentation, LOCI, University of Wisconsin). A similar procedure of Oil Red O staining was performed for THLE2 and mouse derived primary hepatocytes, normalizing the data to the number of nuclei per image.

2.8. Phosphoproteomics

100 mg of the liver of each sample was lysed in 774 μl of a mixture of ice-cold chloroform/methanol (40/60 v/v%) and sodium trimethylsilylpropanesulfonate 254 nmol with a tissue homogenizer (Precellys) in 2 × 30 s cycles at 6000 rpm. Subsequently, 554 μl of a mixture of chloroform/water (45/55 v/v%) was added over the homogenate. Next, the solution was left 15 min in dry ice before being centrifugated for 15 min at 14,000 rpm at 4°C. Then, the two phases obtained were separated at first and then, they were evaporated in a SpeedVac in approximately 3 h. The resulting pellets of both phases were resuspended in 300 μl of each buffer and reference compound. The buffer used for up phase was **Tris-d_{11}-HCl** 100 mM pH 8, NaN_3 1 mM and 100% deuterium oxide (D_2O) whereas this one for down phase was dimethyl sulfoxide-d_6 (DMSO-d_6). Likewise, the reference compound used to up phase was tetramethylphosphonium chloride 1 mM as well as to down phase was triphenylphosphine oxide 4 mM. Likewise, 0.5 mM of Gadobutrol was added over the resuspended solution of the up phase.

All NMR experiments were carried out in a 600 MHz Bruker Avance spectrometer equipped with BBO probehead. For each sample three different experiments were collected: (i) a 1D 31P zgip spectrum with inverse gated 1H decoupling, (ii) a 1D 1H p3919gp with water signals suppression using a binomial 3-9-19 pulse with echo gradient pair, and (iii) a 2D 31P,1H HSQMBC-TOCSY spectrum with coherence selection by gradients. Data processing was done using the TopSpin 4.07 software (Bruker Biospin GmbH). Peaks assignment and quantification were performed as explained in our previous works [22].

2.9. Immunofluorescence

For *O*-GlcNac-Albumin immunofluorescence staining, samples dewax were pre-treated in PTLink Citrate Buffer pH 6. Then, sections were washed three times in TBS 0.1 M for 5 min each and incubated in blocking solution (2% donkey serum + 0.3% Triton X-100 + 0.25% BSA) in TBS 0.1 M for 60 min. Next, sections were incubated with the primary antibodies *O*-GlcNac (ab2739, Abcam) (1:200) and Albumin (ab8940, Abcam) (1:200) in blocking solution for 24 h at 4 °C. After

incubation in the primary antibody, sections were rinsed with TBS 0.1 M three times for 5 min each and then incubated in the solution (0.3% Triton X-100 + 0.25% BSA in TBS 0.1 M) with the secondary antibodies: Alexa 488 anti-mouse (115-545-003, Jackson ImmunoResearch Labs) and Alexa 555 anti-Sheep (A21436, Thermo) 1:1000 for 60 min at room temperature. Sections were then washed and coverslipped with Fluorogel coverslip mounting solution. In all the histological staining, up to 4 representative microphotographs of each animal were taken with a Thunder Imager tissue microscope (Leica Microsystems) (immunofluorescence staining). Leica Las X 3.7.4 software was used for acquisition and analysis of immunofluorescence staining. Image J 1.52p software was used for the quantification of the staining area.

2.10. Mitochondrial membrane potential assessment

The mitochondrial membrane potential was measured using the fluorescent dye tetramethylrhodamine methyl (TMRM). Briefly, mouse primary hepatocytes (6.5×10^3 cells/well) were grown in 12-well chamber slides. 24 h after the treatment with OA, cells were incubated with TMRM 100 nM (#I34361, Invitrogen), and MitoTracker Green 100 nM (#M7514, Invitrogen) for 15 min at 37 °C in the dark. After imaging with confocal microscope, TMRM intensity of fluorescence was quantified with ImageJ 1.52p software and normalized to MitoTracker green fluorescence. Results are the average of 9–11 cells per group.

2.11. Serum levels of metabolites

Whole trunk blood obtained during the sacrifice of mice was collected and then spun for 15 min at 6000×*g* and 4 °C. The supernatant was transferred to a new tube to obtain the serum. Serum alanine transaminase (ALT) activity (41283, Spinreact) were measured by spectrophotometry in a ThermoScientificMultiskan GO spectrophotometer, according to the manufacturer's instructions.

2.12. Human cell cultures

THLE2 human hepatic cell line (American Type Culture Collection, ATCC) was cultured in bronchial epithelial cell basal medium (BEBM) supplemented with a growth factors BulleKit (Lonza/Clonetics Corporation), 70 ng/ml phosphoethanolamine, 5 ng/ml epidermal growth factor, 10% (v/v) FBS and 1% (v/v) Glutamine—Penicillin—Streptomycin solution (MERCK). THLE-2 cells were grown on culture plates pre-coated with a mixture of 0.01 mg/ml fibronectin (#33010018, Sigma Aldrich, USA), 0.01 mg/ml bovine serum albumin (#A4503, Sigma Aldrich, USA) and 0.03 mg/ml collagen type I (#sc-136157, Santa Cruz, USA).

2.13. Isolation and culture of primary hepatocytes

Primary hepatocytes were isolated from male C57BL/6 WT mice via collagenase perfusion. In brief, animals were anesthetized with isoflurane, the abdomen was opened, and a catheter was inserted into the inferior vena cava while the portal vein was cut. Next, liver was washed by perfusion with Krebs-Henseleit (KH) perfusion medium at 37 °C. After the washing, EGTA 0.05% (w/v) was added to the KH medium, and the perfusion was maintained for 5 min. Finally, an enzymatic digestion was performed during 10–12 min with KH perfusion medium supplemented with Ca2+ and 50 mg/ml collagenase type I (LS004196, Worthington). After perfusion, the liver was gently disaggregated. The viable cells were purified by density centrifugation at 500× rpm for 5 min 3 times at 4 °C. Isolated pure hepatocytes were seeded over collagen-coated culture dishes at a density of 4×10^5 cells/well in the medium for cell adhesion (serum-free Dulbecco's modified Eagle's medium (DMEM), supplemented with 10% (v/v) FBS, 1% (v/v) Glutamine—Penicillin—Streptomycin solution and 1% (v/v).

2.14. OGT and *O*-GlcNAcylation silencing and overexpression

All cells were transfected with specific small-interference RNA (siRNA) to knockdown the expression of OGT (siGENOME SMART Pool, Dharmacon). The control group was administered with a non-targeting siRNA (siGENOME Non-Targeting siRNA Pool, Dharmacon). The transfection was performed using Dharmafect 1 reagent (Dharmacon) for THLE2 cells and primary hepatocytes, 0.05 nmol of each siRNA diluted in 250 μl of optiMEM (Life Technologies) was mixed with 6.5 μl for THLE2 and 8 μl for primary hepatocytes of Dharmafect 1; 500 μl of the transfection mixture was added into each well. The medium was replaced with fresh medium after 6 h. Cells were collected after a total of 24 and/or 48 h to check the efficiency of silencing by western blot. The inhibitor OSMI-1 was used at a dose of 100 μM. To enhance *O*-GlcNAcylation, PUGNAc was used, at a dose of 75 μM. To induce NASH features *in vitro*, liver cells were incubated with oleic acid (OA) and methionine and choline deficient medium (MCD, #06-1025-39-1A, Biological Industries). To assess the role of increased levels of UDP-GlcNAc on hepatic lipid accumulation, liver cells were treated with N-Acetyl-D-glucosamine (#A3286, Sigma—Aldrich).

2.15. Oleic acid experiments

In the study with oleic acid, 0.7×10^5 THLE2 and 0.3×10^5 primary hepatocyte cells were seeded in a twenty-four-well plate. Control and OGT-silenced cells were exposed to FBS-free medium supplemented with 1 mM of oleic acid (MERCK) bound to acid-free BSA (Capricorn) at a 2:1 M ratio for 24 h to induce lipid accumulation. Controls were supplemented with fatty acid-free BSA alone. The treatment with oleic acid was added after 24 h of OGT silencing. Cells were stained with Oil Red O to detect lipids.

2.16. Measurement of mitochondrial oxygen consumption rate

The oxygen consumption rate (OCR) of primary hepatocytes was measured at 37 °C by high-resolution respirometry with the Seahorse Bioscience XFp Extracellular Flux Analyzer (Agilent Technologies). For the OCR, measured as the rate change of dissolved O_2, 1.5×10^4 primary hepatocytes were seeded per well in an XFp cell culture microplate (103022-100, Seahorse Bioscience, Agilent Technologies). After 24 h in culture or silencing/overexpression experiments, the medium cells were removed and replaced with pre-warmed assay medium, composed of Seahorse XF DMEM medium (103575-100 Seahorse Bioscience, Agilent Technologies) containing 1 mM sodium pyruvate, 2 mM L-glutamine and 10 mM glucose, and cultured at 37 °C in non-CO_2 incubator. After equilibration in assay medium for 1 h, five basal measurements of OCR were performed. Next, we sequentially added into cells wells the modulators of respiration oligomycin (Oligo, 1.5 μM), carbonyl cyanide-4 (trifluoromethoxy) phenylhydrazone (FCCP, 1 μM) and rotenone/antimycin (Rot/AA, 0.5 μM) (Cell Mito Stress Test Kit, 103010-100, Seahorse Bioscience, Agilent Technologies). The protein content of each well was quantified after the assay to normalize the OCR data. The following key parameters of mitochondrial function were calculated according to the manufacturer's user guide (103011-400, Seahorse Bioscience, Agilent Technologies): basal respiration, ATP-linked respiration, proton leak, maximal respiration, spare capacity and non-mitochondrial oxygen consumption.

2.17. Real-time PCR

RNA was extracted from liver and cells samples using Trizol reagent (Invitrogen) according to the manufacturer's instructions. 100 ng of

total RNA were used for each RT reaction, and cDNA synthesis was performed using the SuperScript First-Strand Synthesis System (Invitrogen) and random primers. Negative control reactions, containing all reagents except the sample were used to ensure specificity of the PCR amplification. For Real-time PCR, we used a fluorescent temperature cycler (Applied Biosystems) following the manufacturer's instructions and SYBR green reagent (Agilent Technologies). The SYBR green cycling conditions included an initial denaturation at 95 °C for 3 min followed by 40 cycles at 95 °C for 5 s and 60 °C for 32 s, with a holding stage of 95 °C for 15 s, 60 °C for 1 min and 95 °C for 15 s. The specific primers used are described in Supplementary Table S3. All reactions were performed in duplicate using the QuantStudio 5 Real-Time PCR (qPCR). Expression levels were normalized to HPRT1 for each sample and the fold change value was determined from the equation $2^{-\Delta\Delta Ct}$.

2.18. Western blot analysis

Total protein lysates from the liver (20 μg) or cells (6 μg) were subjected to SDS-PAGE, electro-transferred onto polyvinylidene difluoride membranes (BioRad) and probed with the antibodies indicated in Supplementary Table S4. For protein detection, horseradish peroxidase-conjugated secondary antibodies and chemiluminescence (Amersham Biosciences) were used. Membranes were exposed to radiograph film (Super RX Fuji Medical XRay Film, Fujifilm) and developed with developer and fixing liquids (AGFA) under appropriate dark room conditions. Protein expression was quantified by densitometric analysis with Image J software. Protein levels were normalized to glyceraldehyde 3-phosphate dehydrogenase (GAPDH) (and HSP90 only for OXPHOS analysis) for each sample and expressed in relation to the control group.

2.19. Quantitative mass spectrometry bases *O*-GlcNAcylation immunoprecipitation using SWATH method

For the immunoprecipitation assay, protein extracts from liver were incubated overnight at 4 °C with control IgG (m-IgG2a. sc-542731, Santa Cruz Biotechnology) or specific primary antibody (*O*-GlcNAc, ab2739, Abcam). Antibodies were precipitated with Protein G Agarose beads (Protein G Sepharose 4 Fast Flow. 17-0618-01, GE Healthcare). The captured proteins were centrifuged, the supernatants discarded, and the beads were washed in lysis buffer. Lysis buffer contained Pugnac 10 μM (Sigma), streptozotocin (STZ) 2 mM (Sigma), Thiamet-G (TMG) 10 μM (Sigma) and GlcNAc 40 mM (Sigma) to preserve the integrity of *O*-GlcNAcylated proteins (Cuifang Han, Nature Communications 2017). Buffer lysis was also supplemented with TritonX 1%. Proteins from the immunoprecipitation were loaded on a 10% SDS-PAGE gel to whole-protein in gel concentration. Gel was staining and the band was exscinded and submitted to an in gel tryptic digestion [13]. Peptides were extracted by carrying out three 20-min incubations in 40 μl of 60% acetonitrile dissolved in 0.5% HCOOH, then pooled, concentrated (SpeedVac), and stored at −20 °C. Mass spectrometric analysis by SWATH (SequentialWindow Acquisition of all Theoretical Mass Spectra). In order to construct the MS/MS spectral libraries each sample was equally pooled in the correspondent groups. All peptide solutions were analyzed by a shotgun data-dependent acquisition (DDA) approach by micro-LC-MS/MS, an analysis already described previously in the literature [14–16]. Therefore, ion density found in the DDA runs was used to create the necessaries windows in the SWATH method. Once the SWATH method is created, the individual samples were run as described previously by our group [15,16]. The targeted data extraction from the SWATH runs was performed by PeakView (version 2.2) using the SWATH Acquisition MicroApp (version 2.0) and the data was processed using the spectral library created previously from DDA runs. SWATH quantization was attempted for all proteins in the ion library that were identified by ProteinPilot with an FDR below 1%. PeakView computed an FDR and a core for each assigned peptide according to the chromatographic and spectra components; only peptides with an FDR below 1% 10 peptides and 7 transitions per peptide were used for protein quantization.

The integrated peak areas were processed by MarkerView software (AB SCIEX) for data-independent method for relative quantitative analysis [15,16]. To control for possible uneven sample loss across the different samples during the sample preparation process, we performed an MLR (Most Likely Ratio) normalization [17,18]. Unsupervised multivariate statistical analysis using principal component analysis (PCA) was performed to compare the data across the samples. A Student's t-test analysis on the averaged area sums of all the transitions derived for each protein in every sample will indicate how well each variable distinguishes the two groups, reported as a p-value. For each library, each set of differentially expressed proteins (p-value <0.05) with a 1.2-fold was selected. Functional analysis was performed using the online Reactome software and FunRich3.1.3 software (Functional Enrichment Analysis Tool). Volcano plots were performed using GraphPad Prism 8.0.2, and the heatmap was performed using the online Heatmapper software (Wishart Research Group, University of Alberta).

2.20. Statistical analysis

Data are expressed as mean ± standard error mean (SEM) or standard deviation (SD), as indicated. Statistical significance was determined by two-tailed Student's t-test or Mann–Whitney test when two groups were compared or One-way ANOVA with Bonferroni or Newman–Keulspost tests when more than two groups were compared. The significance level was set at $p < 0.05$. GraphPad Prism Software 6.01 was used to compute the statistical analyses and graphics. To study the correlation between O-GlcNAcylation levels and different parameters in human patients, Gaussian distribution of data was assessed by Shapiro–Wilk test. Then, Pearson's (parametric) or Spearman's (nonparametric) correlation coefficient (r) was calculated.

3. RESULTS

3.1. *O*-GlcNAcylation is increased in patients and rodents with liver fibrosis

We found that protein levels of OGT were significantly higher in liver samples from patients with NASH and liver fibrosis than from healthy individuals (Figure 1A). In addition, immunofluorescence labeling in liver sections showed that *O*-GlcNAcylation colocalized with albumin (a marker of hepatocytes) in NASH liver but not in healthy liver (Figure 1B). *O*-GlcNAcylation showed a positive correlation with steatosis stage, fibrosis stage and NAS score (Figure 1C). Hematoxylin and eosin staining and Masson's trichrome staining in the different groups are shown in Figure S1.

Next, we evaluated OGT levels in the liver and isolated hepatocytes from two mouse models of diet-induced NASH: i) mice fed a MCD diet (MCDD) for 4 weeks, and ii) mice fed a CD-HFD for one year (Figure 2A and B). Each of these animal models displayed consistently elevated protein levels of OGT in the whole liver (Figure 2C and F). To note, OGT was already increased after 3 and 12 weeks on CD-HFD (Figure 2A). OGT mRNA levels were also higher in isolated hepatocytes of mice fed a MCDD and CD-HFD (Figure 2D and G). Using metabolomics, we measured UDP-GlcNAc and UDP-GalNAc (which is also supplied by hexosamine biosynthetic pathway and is generated by the

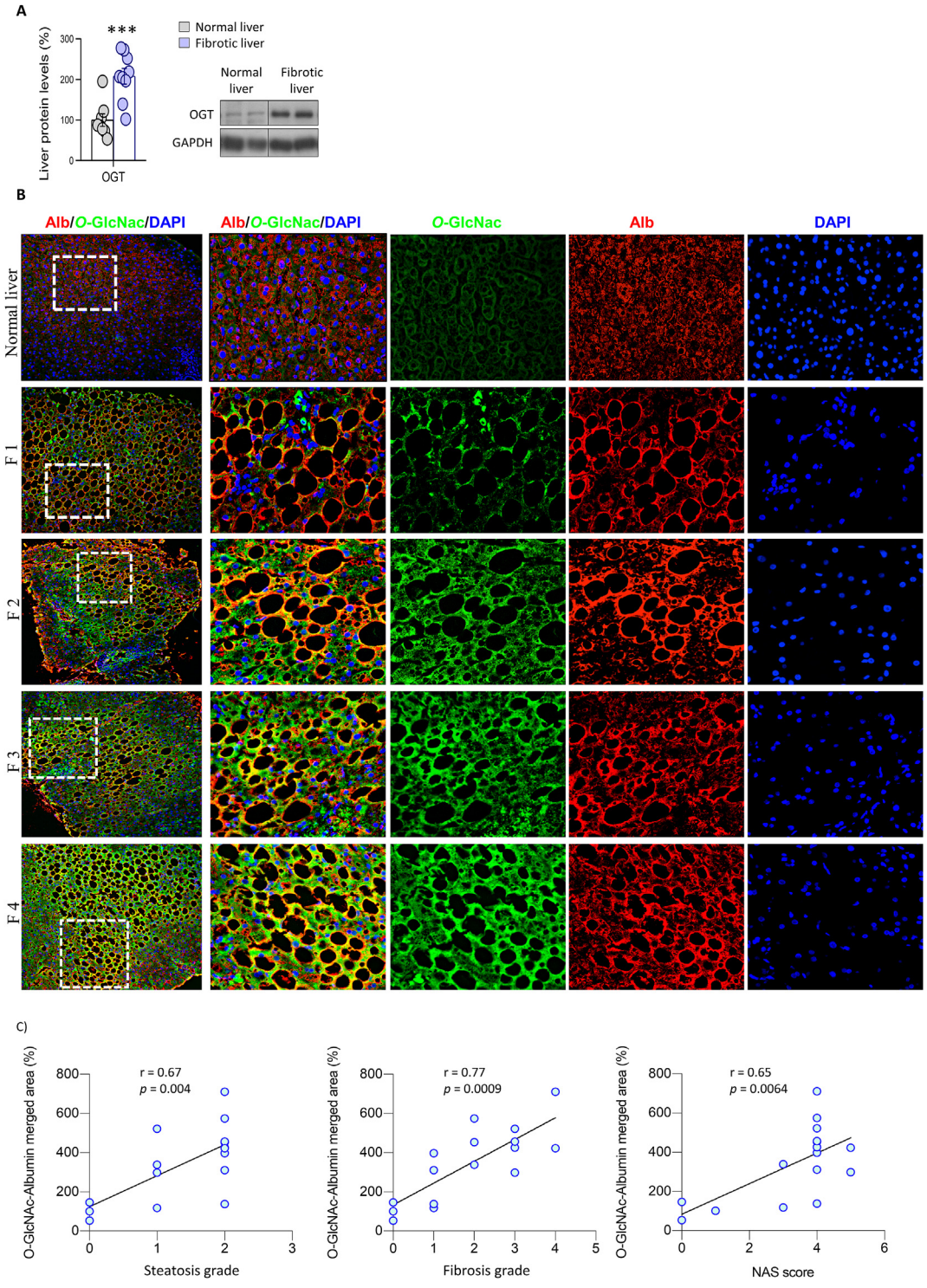

Figure 1: *O*-GlcNAcylation is upregulated in the hepatocytes of patients with liver fibrosis. A) OGT protein levels in healthy individuals and patients with NASH and fibrosis (n = 8–9). B) Representative colocalized immunofluorescence for albumin (red) with *O*-GlcNAc (green) in healthy (normal liver) and patients with NASH and fibrosis. Nuclei were stained with DAPI (blue). C) Correlations of albumin-*O*-GlcNAc merged area with the steatosis score, fibrosis score and NAFLD activity score (NAS) are shown (Spearman correlation) (n = 14–16). ***p < 0.001, using a two-tail Student's *t*-test (A).

epimerization of UDP-GlcNAc) and found that these metabolites were increased in the liver of both animal models with liver fibrosis (Figure 2E and H). In agreement with this, higher levels of *O*-GlcNAcylation were also detected in hepatocytes of mice fed a MCDD and CD-HFD (Figure 2I; measured as the *O*-GlcNAc-albumin merged area). These changes were independent of protein levels of OGA, since they remained unchanged in the liver of mice fed a CD-HFD or MCDD (Figure S2B–S2C). Thus, these findings indicate that *O*-GlcNAcylation

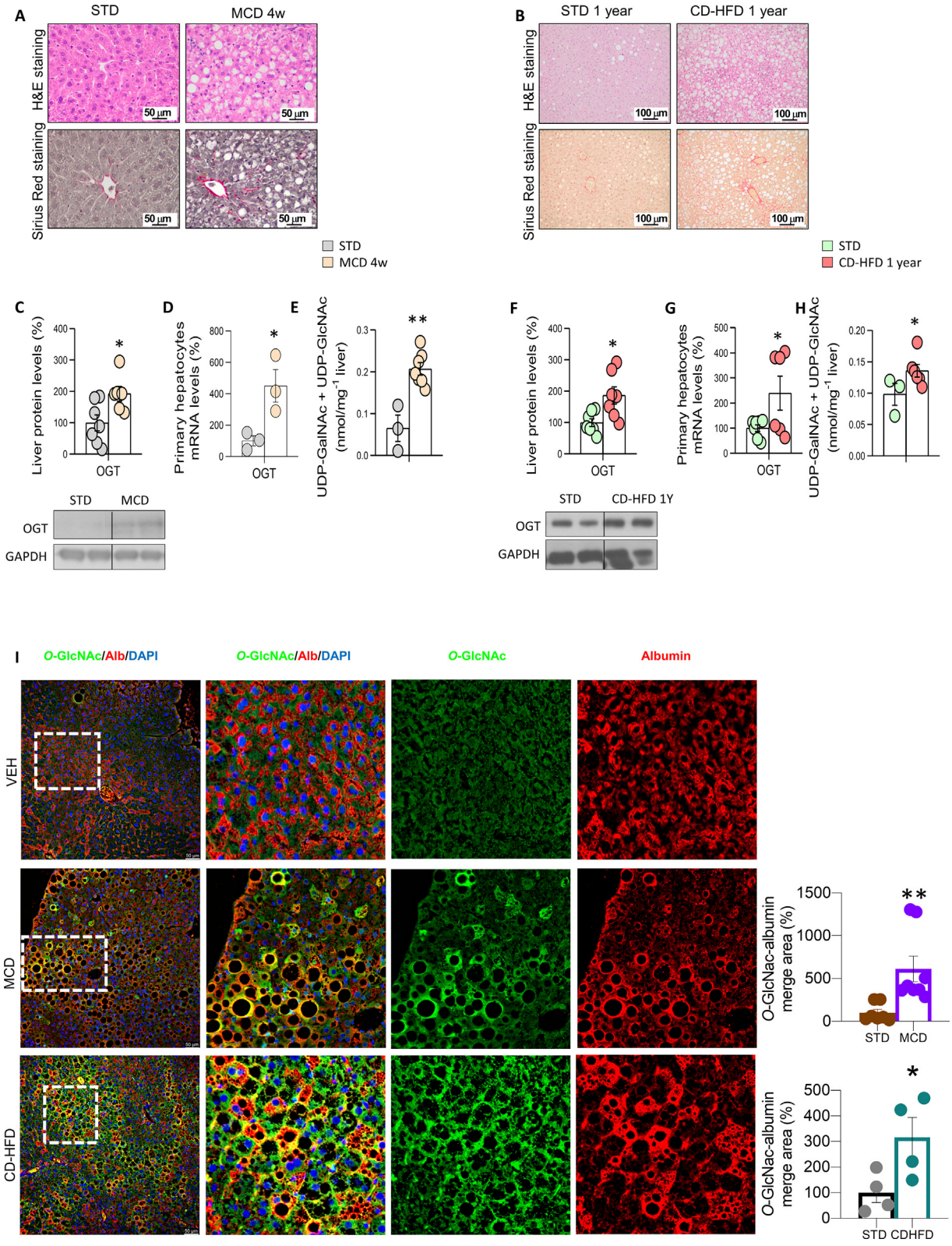

Figure 2: *O*-GlcNAcylation is increased in *in vivo* preclinical models of liver fibrosis. Mice were fed: A) a standard diet (STD) or a metionine- and choline-deficient diet (MCD diet) for 4 weeks; or B) a choline-deficient high-fat diet (CD-HFD) for one year. Representative microphotographs are shown of hematoxylin and eosin staining (H&E; upper panel) and Sirius red staining (lower panel) of liver sections. Expression of OGT in samples of total liver (C and F) and isolated primary hepatocytes (D and G) of each of the models ($n = 3–7$). Levels of UDP-GalNAc and UDP-GlcNAc (E and H) in the liver of both animal models ($n = 3–7$). I) Representative immunofluorescence for *O*-GlcNAc in the liver of each of the *in vivo* models. Quantification of albumin-*O*-GlcNAc merged areas are also shown for each of the models ($n = 4–8$). *$p < 0.05$, **$p < 0.01$ using a two-tail Student's *t*-test (C–I).

is increased in patients as well as in preclinical mouse models of severe NASH.

3.2. OGT-downregulation in the liver alleviates liver injury in animal models of NASH

We next investigated whether the increased *O*-GlcNAcylation in liver injury could be the cause or consequence of the disease. For this, we downregulated OGT in mouse models of induced liver fibrosis. In the MCD diet model, wild-type (WT) mice were injected with a lentivirus encoding luciferase (sh-luciferase, as a control) or an shRNA against OGT (shOGT) and then fed a standard diet (STD) or MCD diet for one month (Figure 3A). The protein levels of hepatic OGT were decreased after the lentiviral injection (Figure 3A). As expected, mice fed a MCD showed a reduced body weight compared to STD-fed mice, but no differences were observed between MCD+sh-luciferase and MCD+shOGT mice (Figure 3B). Hepatic knockdown of OGT reduced the high circulating levels of ALT induced by MCD (Figure 3C). Consistent with this, MCD-fed mice with OGT-knockdown showed reduced levels of the stained areas with Sirius red (to show liver fibrosis) and Oil Red O (for hepatic lipid content) and of collagen type I content in liver sections as compared to control mice fed the same diet (Figure 3D). Moreover, MCD-fed mice with OGT-knockdown displayed reduced expression in the liver of mRNA encoding fibrogenic markers of collagen type alpha 1 (Col1α1), collagen type alpha 2 (Col1α2), and smooth muscle α actin (Acta2), as well as of mRNA encoding inflammation markers, such as tumor necrosis factor α (TNF α), transforming growth factor beta (TGFβ), interleukin 6 (IL6), and F4/80-positive macrophages (Figure 3E and F).

We also performed a second experiment in mice fed a MCDD, but this time we first injected lentivirus encoding a sh-luciferase or shOGT, and 30 days later we fed the mice with STD or MCD diet for another 30 days (Figure S3A), following a prevention strategy. In this experiment, we also found that body weight was reduced by MCD diet but without no differences between MCD+sh-luciferase and MCD+shOGT mice (Figure 3B). The inhibition of OGT in the liver was also able to improve the liver status, since the high levels of circulating ALT (Figure 3C), collagens (Figure 3D), liver fatty acid content (Figure 3D) and mRNA expression of fibrotic and inflammatory markers (Figure S3E–S3F) detected in the liver of mice fed a MCD diet were significantly reduced after the knockdown of OGT in the liver.

In the CD-HFD model, mice were fed a CD-HFD (for a total of 12 weeks) and injected at week 8 with a lentivirus encoding a sh-luciferase or (shOGT Figure 3G). Similar to the previous experiment, the hepatic knockdown of OGT lowered circulating ALT levels (Figure 3H), Sirius red-stained areas, hepatic lipid and collagen type I content (Figure 3I) and the mRNA expression of fibrogenic and inflammatory markers (Figure 3J–K). Overall, these results indicate that impairing *O*-GlcNAcylation in liver protects against fibrosis development. To note, these effects were not associated with changes in endoplasmic reticulum stress, which was markedly increased in our mouse model of diet-induced liver damage, but remained high after the inhibition of OGT (Figure S3G and S4A). The improvement of liver status was also independent of cellular proliferation or apoptosis, since in all animal models, the immunostaining of cleaved caspase 3 (CC3) and Ki67 remained unchanged between control and OGT-knockdown mice (Figure S4B–S4C).

To note, we have also investigated the effects of the inhibition of OGT in WT mice fed a chow diet. In agreement with previous reports [23], we found that the down-regulation of OGT has a detrimental role in healthy mice (Figure 5), highlighting the relevance of maintaining *O*-GlcNAcylation within the optimal physiological range to maintain liver proper functioning, since excess and defect are both prejudicial.

3.3. The specific inhibition of OGT in hepatocytes protects against liver injury in models of NASH

Since downregulation of OGT in the whole liver effectively ameliorated fibrosis, we tested whether the specific ablation of OGT in hepatocytes would be sufficient to reproduce the results. For this, C57BL/6J mice expressing Cre recombinase under the control of the albumin gene promoter with α-fetoprotein enhancer (Alfp-Cre) were injected into the tail-vein with AAV8-FLEX-GFP (control) or AAV8-FLEX-shOGT, and were fed a MCD diet for 4 weeks. Mice with an OGT-knockdown specifically in hepatocytes had lower protein levels of hepatic OGT (Figure 4A) and reduced levels of *O*-GlcNAcylation in hepatocytes as shown by the *O*-GlcNAc signal specifically reduced in Alfp-Cre mice fed a MCD and treated with AAV8-FLEX-shOGT (Figure 4B). Mice with an OGT-knockdown specifically in hepatocytes also displayed a similar phenotype to those with an OGT-knockdown in all liver cell types. Circulating ALT, Sirius red area, lipid and collagen staining and gene expression of markers for fibrosis and inflammation were reduced in mice lacking OGT in hepatocytes as compared to the control mice (Figure 4C–F). Again, these effects were not related to cellular proliferation or apoptosis, as the immunostaining of Ki67 and CC3 was similar between AAV8-FLEX-shGFP and AAV8-FLEX-shOGT (Figure 4G).

3.4. Inhibition of *O*-GlcNAcylation reduces lipid content in hepatocytes

To further assess the relevance of OGT expression in the hepatocytes during NASH, primary mouse hepatocytes were isolated from mice fed a standard chow diet and then were incubated in a control or a MCD medium, which induces steatosis and injury [24]. Primary hepatocytes were also treated with OA, a well-known condition of inducing lipid accumulation and lipotoxicity [25]. Protein levels of OGT were significantly elevated when incubated in a MCD medium or with OA (Figure S6A and S6B). Consistent with this, exposure of cells of the human liver cell line THLE-2 to these two conditions also induce higher levels of OGT (Figure S6C and S6D). Given that OA induced the expression of OGT, we next assessed whether the inhibition of OGT could ameliorate the effects of fatty acids. For this, primary hepatocytes were first treated with OA and then incubated with OSMI-1, a small-molecule inhibitor of OGT that decreases *O*-GlcNAcylation levels [26]; in another group of hepatocytes, OGT was genetically silenced. Both pharmacological and genetic inhibition of OGT reduced OA-induced lipid accumulation (Figure S6E and S6F). In agreement with this, down-regulation of OGT also protected THLE-2 cells against OA-induced effects (Figure S6G and S6H).

We next isolated hepatocytes from mice fed a standard chow diet or CD-HFD for 52 weeks. Primary hepatocytes isolated from CD-HFD–fed mice displayed higher protein levels of OGT (Figure 5A). Genetically silencing OGT in these primary hepatocytes reduced the CD-HFD–induced lipid storage, as observed by reduced Oil Red O staining (Figure 5B). Similar results were obtained when hepatocytes isolated from CD-HFD–fed mice were incubated with OSMI-1 (Figure 5C). Further, genetically silencing of OGT from primary hepatocytes from mice fed a MCD diet for 4 weeks reduced the amount of lipids as compared to the control (hepatocytes from mice fed a standard chow diet), as observed by Oil Red O staining (Figure 5D). Similar results were obtained when hepatocytes isolated from MCD diet-fed mice were incubated with OSMI-1 (Figure 5E). Overall, these results

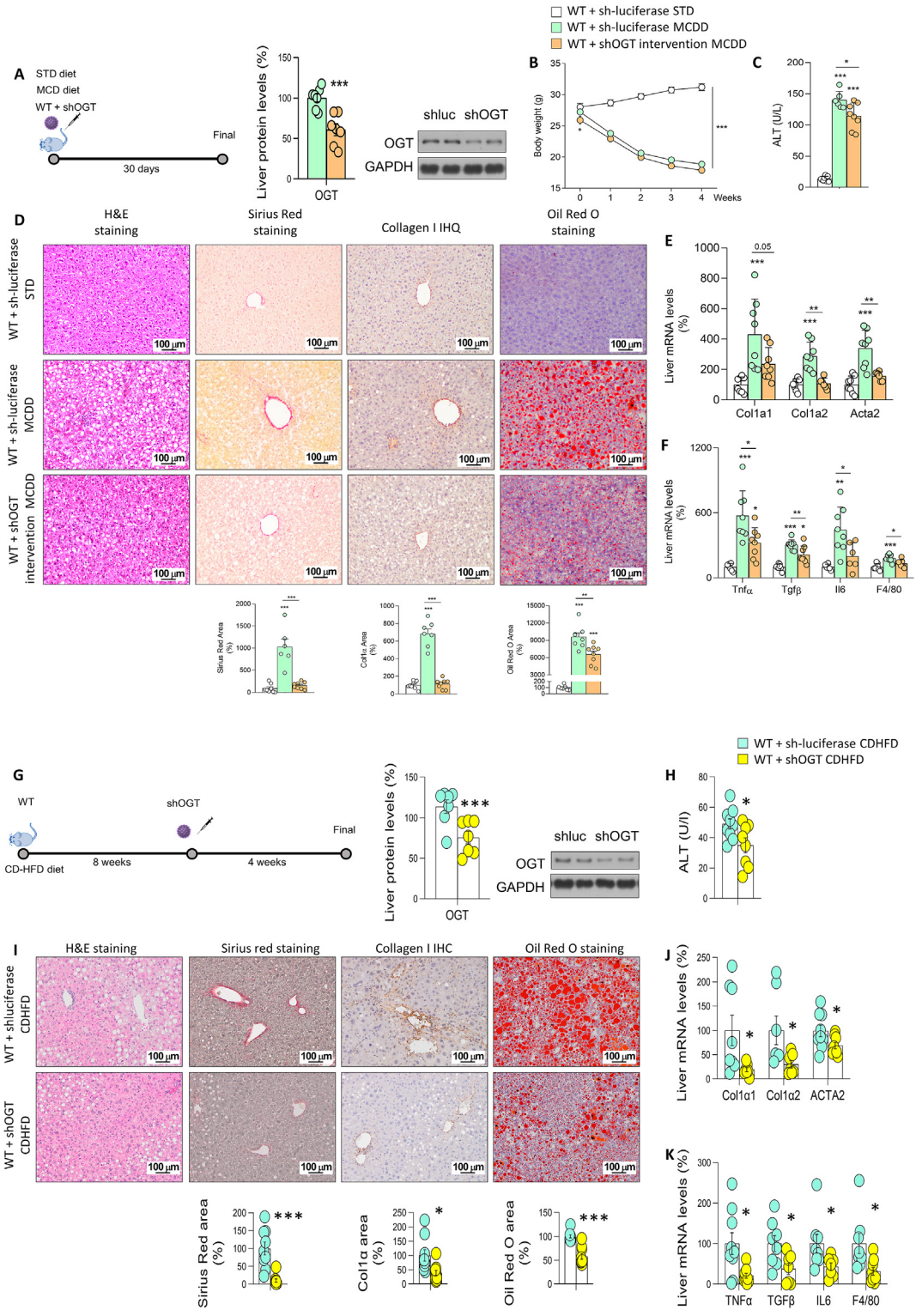

Figure 3: OGT inhibition ameliorates MCD- and CDHFD-induced hepatic fibrosis. A) OGT inhibition in wild-type (WT) mice fed a MCD diet compared to mice fed a standard diet (STD) and analysed by: B) Body weight of mice; C) ALT; D) hematoxylin & eosin, Sirius red, collagen 1 and Oil Red O staining. E, F) Expression of fibrosis (E) and inflammation (F) markers in mice injected with sh-luciferase or shOGT and fed a MCD diet ($n = 6–8$). G) OGT inhibition in WT mice fed a CDHFD and analysed by: H) ALT; I) hematoxylin & eosin, Sirius red, collagen 1 and Oil Red O staining. J, K) Expression of fibrosis (J) and inflammation (K) markers in mice injected with sh-luciferase or shOGT and fed a CDHFD ($n = 7–10$). *$p < 0.05$, **$p < 0.01$, ***$p < 0.001$, using a two-tail Student's *t*-test (A), (G–K) or one-way ANOVA followed by a Bonferroni multiple comparison test (B–F).

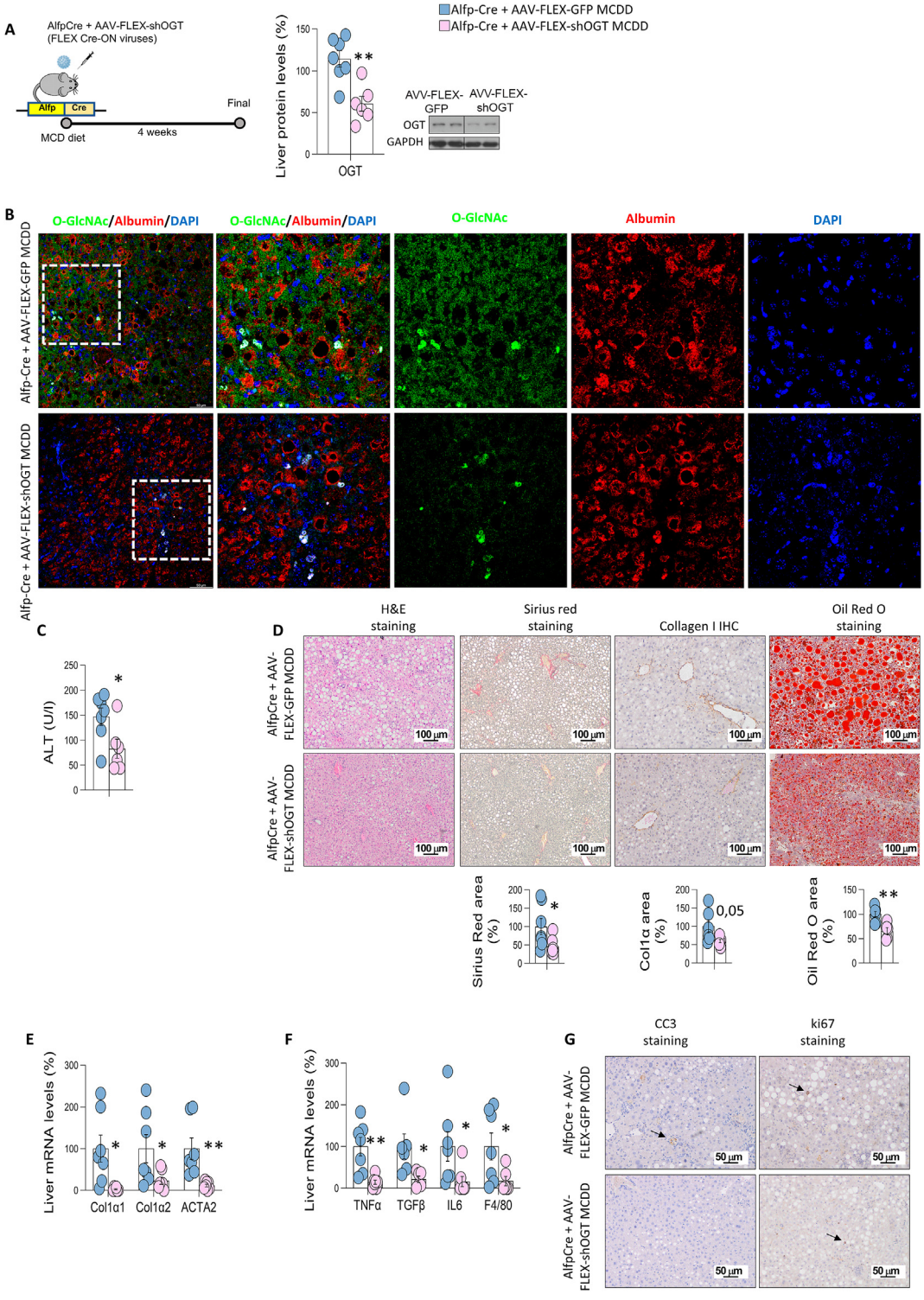

Figure 4: Specific OGT deficiency in hepatocytes protects against liver fibrosis. A) Protein levels of OGT after its inhibition in MCD diet-fed Alfp-Cre mice using AAV-FLEX viruses. B) Representative colocalized immunofluorescence for albumin (red) with *O*-GlcNAc (green) in control (Alfp-Cre+AAV-FLEX-GFP) and mice with OGT knockdown (Alfp-Cre+AAV-FLEX-shOGT). Nuclei were stained with DAPI (blue). C) ALT levels. D) hematoxylin & eosin, Sirius red, collagen 1 and Oil Red O staining; E, F) Expression of fibrosis (E) and inflammation (F) markers in mice Alfp-Cre mice injected with AAV-FLEX-GFP or AAV-FLEX-shOGT and fed a MCD diet ($n = 5–7$). G) Representative microphotographs are shown of cleaved caspase 3 (CC3) and ki67 staining of liver sections. *$p < 0.05$, **$p < 0.01$, ***$p < 0.001$, using a two-tail Student's *t*-test (A—F).

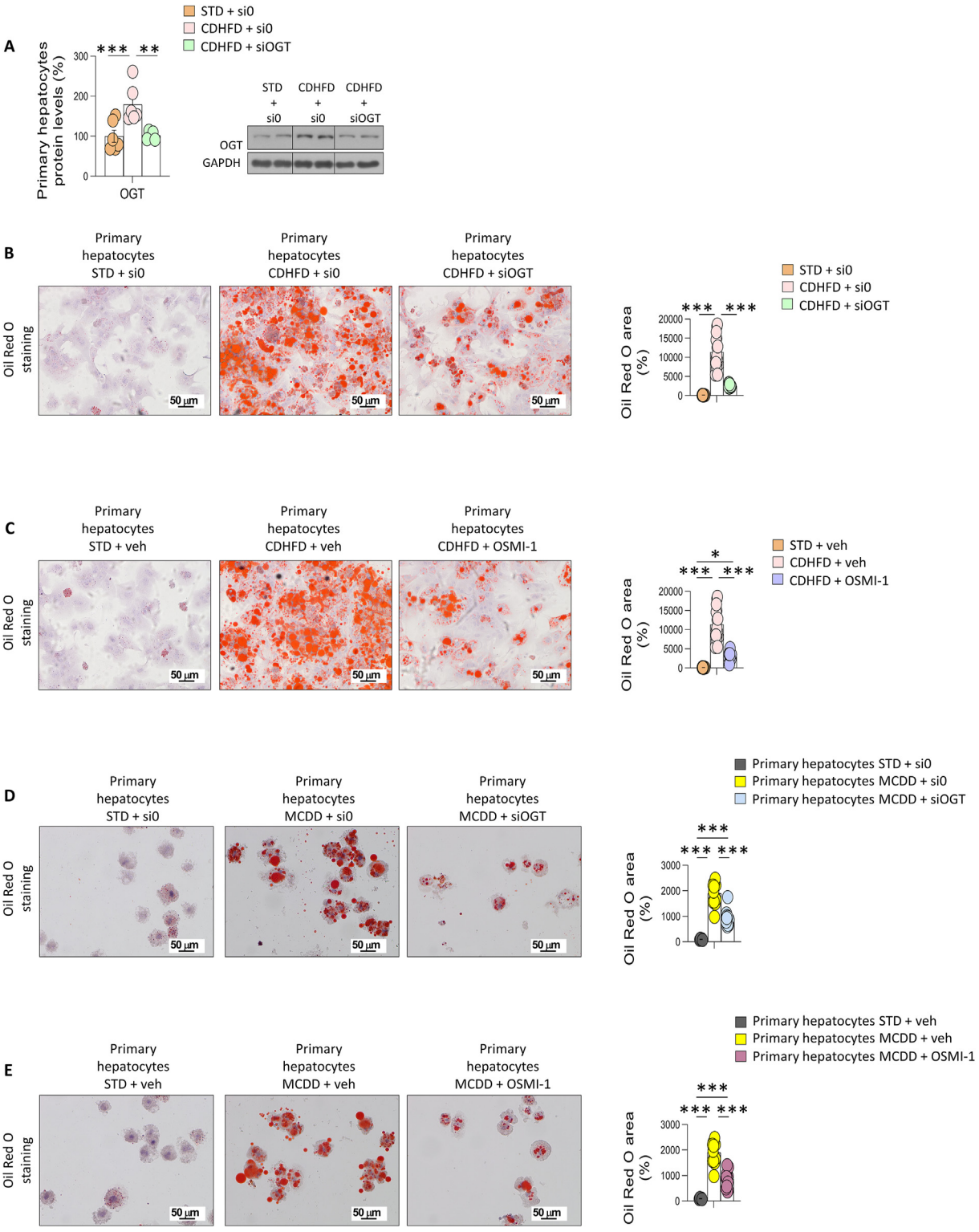

Figure 5: Specific OGT inhibition in hepatocytes reduces hepatic lipid content in *in vitro* models of liver fibrosis. A–C) OGT protein levels and Oil Red O staining in primary hepatocytes from mice fed standard diet (STD) and CDHFD, and treated with empty siRNA, siRNA-OGT, vehicle, and/or the *O*-GlcNAcylation inhibitor OSMI-1, as indicated. D, E) Oil red O staining in primary hepatocytes from mice fed standard diet (STD) and MCD, and treated with empty siRNA, siRNA-OGT, vehicle, and/or the *O*-GlcNAcylation inhibitor OSMI-1, as indicated. Quantification of Oil Red O area is also shown (n = 5–16). *p < 0.05, **p < 0.01, ***p < 0.001, using a one-way ANOVA followed by a Bonferroni multiple comparison test.

indicated that OGT was augmented when hepatocytes store abnormal amounts of fatty acids, and the selective inhibition of this protein prevented lipid accumulation.

To study whether *O*-GlcNAcylation was sufficient to induce steatosis, we treated primary hepatocytes from control-diet mice with O-(2-acetamido-2-deoxy-D-glucopyransylidene)-amino-N-phenylcarbamate (PUGNAc), an inhibitor of OGA that increases protein *O*-GlcNAc levels [27]. Our data showed that the pharmacological induction of *O*-GlcNAcylation increased the lipid content in hepatocytes (Figure 7A). In line with this, PUGNAc also increased the content of fatty acids in THLE-2 cells (Figure 7B). To further corroborate these findings, we treated THLE-2 cells with glucosamine, which increased hepatic lipid content in a dose-dependent manner (Figure 7C). Strikingly, this effect was blunted when OGT was genetically silenced, highlighting that increased glucosamine affects hepatic lipid accumulation mainly through *O*-GlcNAcylation (Figure 7D). Taken together, our results suggested that activation of *O*-GlcNAcylation may have a causal effect in inducing steatosis.

3.5. Mitochondrial proteins are *O*-GlcNAcylated upon liver fibrosis

O-GlcNAcylation is a PTM that affects to numerous proteins. To investigate which hepatic proteins could be *O*-GlcNAcylated in mice with fibrosis, we used livers from mice fed a MCD diet or CD-HFD. The samples were immunoprecipitated with an anti-*O*-GlcNAc antibody, and the content was used to perform proteomics (Figure 6A). Using an unbiased proteomics approach, we found that multiple changes in hepatic protein *O*-GlcNAcylation were associated with severe NASH. Specifically, we detected more than 850 proteins whose *O*-GlcNAcylation is altered under diet-induced NASH, as it is shown in the Volcano Plot (Figure 6B). Given that we have previously demonstrated that *O*-GlcNAcylation is hyper activated upon liver damaged, we focused on those proteins whose *O*-GlcNAcylation is increased under NAFLD conditions compared to STD fed mice (82 proteins in CD-HFD and 138 proteins in MCD diet), and looked at those commonly modified in both CD-HFD and MCD diet experiments (36 proteins), to find out a common mechanism linking OGT hyperactivation, increased *O*-GlcNAcylation and liver injury (Figure 6B). Of these 36 shared proteins, 20 are related to metabolic functions, with mitochondria identified as the most affected cell component (Figure 6C). A heatmap showed several mitochondrial proteins with a strong *O*-GlcNAcylation upon fibrosis (Figure 6D).

Taking into account the important role of mitochondrial function in fatty acid metabolism [28], we next investigated if changes in global *O*-GlcNAcylation affect mitochondrial activity. For this, we measured mitochondrial respiration and glycolytic flux in primary hepatocytes incubated with OA or in MCD medium and with or without genetic or pharmacological inhibition of OGT; note that these conditions that induce cell stress, OGT expression, and hepatic lipid accumulation, as shown before (Figure S6A–H). As expected, mitochondrial respiration was markedly reduced by OA and MCD (Figure S8A–D). However, silencing OGT completely restored mitochondrial activity (Figure S8A–D) which is in line with the reduced lipid content caused after the inhibition of OGT (Figure S6E–H and Figure 5). Similar results were obtained when OGT was pharmacologically inhibited with OSMI-1, which blunted OA-induced mitochondrial dysfunction (Figure 7A and B). In line with the results on mitochondrial respiration, OA reduced protein levels of complex II and V, while OSMI-1 restored the expression of those mitochondrial complexes to basal level (Figure 7C). Finally, we performed a TMRM assay to measure the mitochondrial membrane potential and found that the damage caused by OA in the membrane potential was reestablished after the treatment with OSMI-1 (Figure 7D).

To finally demonstrate the role of *O*-GlcNAcylation in mitochondrial activity, we treated primary hepatocytes with PUGNAc, a pharmacological activator of *O*-GlcNAcylation, and detected a significant reduction in mitochondrial respiration after 6 and 24 h (Figure S9A and B). Altogether, these data indicate that *O*-GlcNAcylation induces mitochondrial dysfunction while its inhibition stimulates mitochondrial activity, contributing to cell dysregulation under conditions of hepatic injury.

4. DISCUSSION

In this work, we describe that *O*-GlcNAcylation is involved in the pathogenesis of NAFLD progression. *O*-GlcNAcylation is elevated in the liver of NASH animal models as well as in patients with NAFLD. *In vitro* and *in vivo* genetic functional studies indicated that inhibition of OGT, the enzyme that catalyzes the transfer of *O*-GlcNAc, alleviates liver injury in different mouse models and reduces the lipid content in hepatocytes. These effects are mediated by the improvement of the mitochondrial dysfunction caused by excess lipid accumulation.

O-GlcNAcylation of a large variety of proteins has been found to be elevated in human NAFLD-induced HCC tumor tissues [17] and participates in the development of liver cancer that is not related to NAFLD [29–33]. However, another study reported decreased *O*-GlcNAcylation levels in patients with alcoholic liver cirrhosis and in mice with ethanol-induced liver injury [23]. In the current study, results obtained in patients and three different mice models with steatohepatitis and fibrosis point all to the same direction, of *O*-GlcNAcylation being markedly increased as compared to healthy controls. Therefore, our results are in agreement with a deleterious effect that aberrant *O*-GlcNAcylation may have on the progression of NASH to HCC. The lower *O*-GlcNAcylation levels found in alcoholic-induced cirrhosis could be likely explained by the strong differences in the molecular underpinnings leading to NASH and alcoholic-induced cirrhosis. As a matter of fact, one study reported that there were more proteins involved in tumorigenesis in alcoholic steatohepatitis (ASH) than in NASH [34].

In this work, OGT was downregulated in the whole liver as well as specifically in hepatocytes in different mouse models under conditions of liver injury. Of note, OGT downregulation displayed a protective phenotype against diet-induced severe NASH, suggesting again that *O*-GlcNAcylation is involved in the progression of liver damage. A previous study reported that mice with hepatocytes deficient for OGT progress to liver fibrosis and portal inflammation when fed a standard chow diet [23]. Indeed, when we analyzed the liver of our mouse models fed a chow diet after four weeks, we also found a significant increase in hepatic lipid content. Therefore, the deletion of OGT exerts very different actions in mice depending on the liver status: it is detrimental when they are in a normal condition, but beneficial when they have severe NASH. To reconcile the diverse functions and effects of *O*-GlcNAcylation, it is important to consider the concept of *O*-GlcNAc homeostasis, which occurs only at certain cellular *O*-GlcNAcylation levels within the safe (homeostatic) limits. A minimum level of *O*-GlcNAcylation would be present to ensure *O*-GlcNAcylation of target proteins for their proper functions, since lack of *O*-GlcNAcylation would impair the structural integrity of protein substrates and their essential roles. However, hyper-*O*-GlcNAcylation, as a result of hyper-OGT activity or high UDP-GlcNAc levels, would result in persistent *O*-GlcNAcylation of target and off-target proteins, leading to cell malfunction [11,35]. The results presented in this study constitute an example of

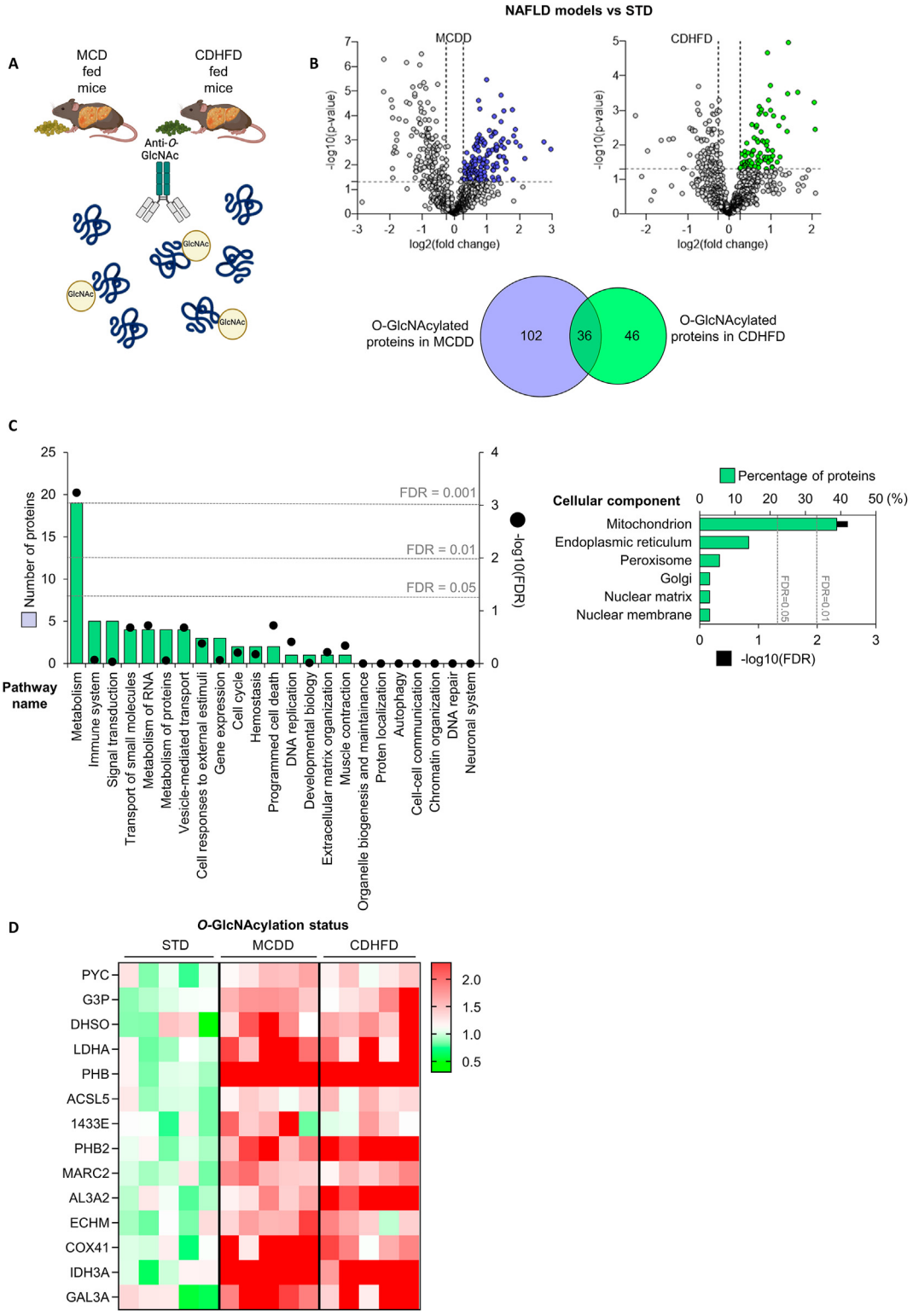

Figure 6: Mitochondrial proteins are hyper-*O*-GlcNAcylated in *in vivo* models of liver fibrosis. A) Schematic representation of the immunoprecipitation procedure. B) Volcano plots and Venn diagram of the *O*-GlcNAcylated proteins from the livers of MCD diet- or CDHFD-fed mice. C) Reactome pathway classification of shared *O*-GlcNAcylated proteins from the liver of mice from (B), showing the number of proteins included in each category and the associated FDR. The same proteins were also classified according to the cellular component using FunRich tool. D) Heatmap representation of immunoprecipitated *O*-GlcNAcylated proteins in the liver of mice fed a STD, MCD diet or CDHFD.

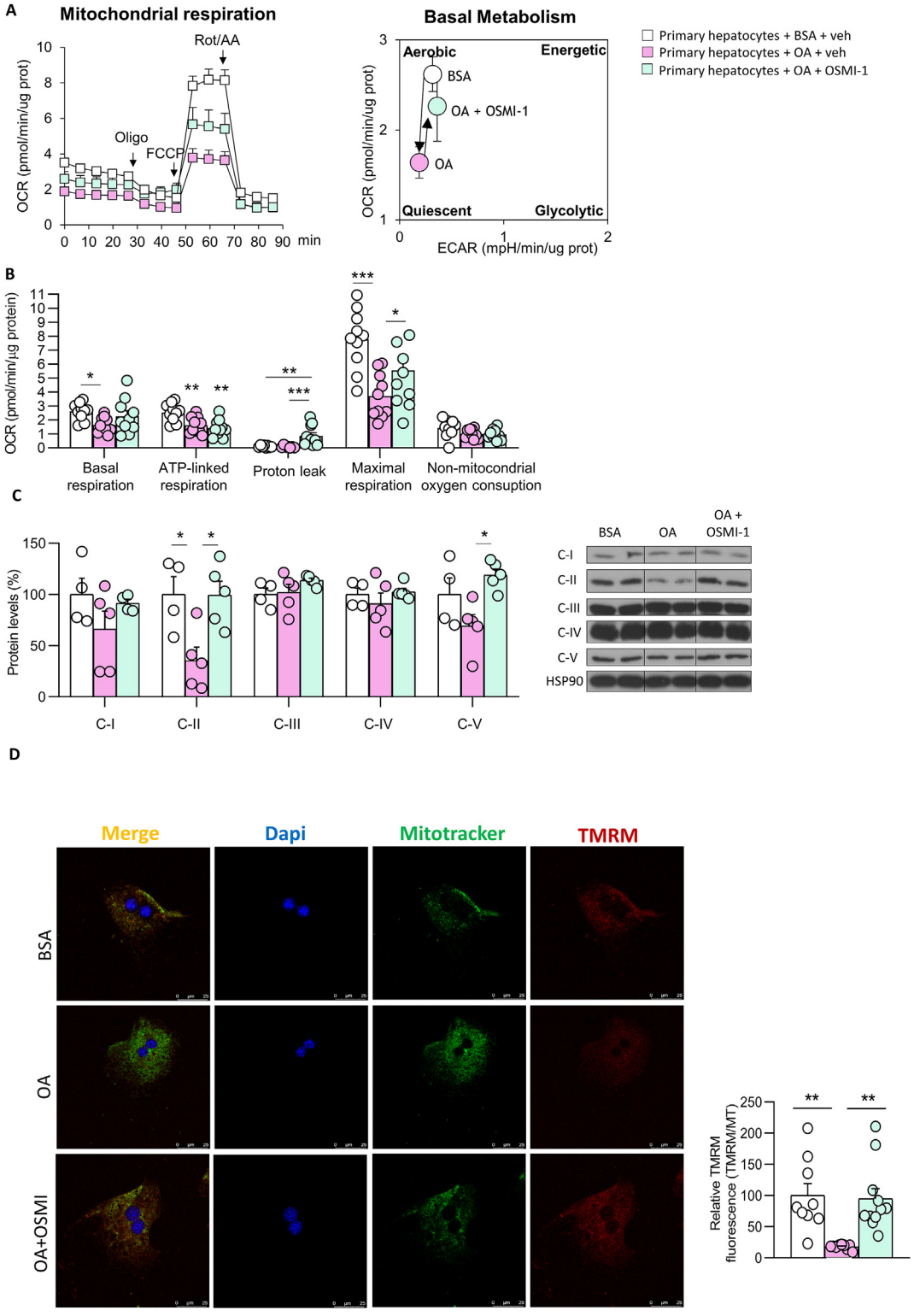

Figure 7: *O*-GlcNAcylation affects mitochondrial activity in *in vitro* models of liver fibrosis. A) Oxygen consumption rate (OCR) in primary hepatocytes treated with BSA or oleic acid (OA) and then incubated with OSMI-1. Arrows indicate the timepoint at which mitochondrial respiration modulators (oligomycin [Oligo], phenylhydrazone [FCCP], or rotenone/antimycin A [Rot/AA]) were added to the assay. Right, graph depicting the effects of OA or OA+OSMI-1 on aerobic or quiescent metabolic states, based on quantification of glycolysis and oxygen consumption rate during basal metabolism. B) Parameters of mitochondrial function ($n = 10$). C) Protein levels of OXPHOS complexes ($n = 4–5$). D) TMRM and MitoTracker immunostaining ($n = 9–11$). $^{**}p < 0.01$ and $^{***}p < 0.001$, using a one-way ANOVA followed by a Bonferroni multiple comparison test.

the effects that deregulation of *O*-GlcNAcylation can generate, leading in this case to the development of NASH. Deregulation of OGT activity led to the hyper-*O*-GlcNAcylation of proteins that are not modified under control-STD-conditions, as we can see by our proteomic assay. Furthermore, many of the *O*-GlcNAcylated proteins were distinct in mice fed a MCD diet or a CD-HFD, compared to STD fed mice. This means that OGT downregulation in NASH (when *O*-GlcNAcylation is elevated) will affect to the stability and/or function of proteins that are functioning normally in a healthy condition.

Another difference between the previous study and our two mouse models (e.g., knockdown of OGT in the whole liver or specifically in hepatocytes) is that we performed inhibition at adult stages, while the previous work deleted OGT at embryonic stages [23]. This could be initially relevant because *O*-GlcNAcylation is essential in embryonic viability and for mouse ontogeny, with germline OGT deletion lethal at the embryogenesis stage [36]. However, the fact that we observed that knockdown of OGT in adult mice fed a chow diet also developed liver steatosis indicates that OGT disruption in embryonic or adulthood stages lead to similar deleterious hepatic action.

A key aspect to understanding how *O*-GlcNAcylation works upon liver damage is to analyze which proteins are *O*-GlcNAcylated. Our data indicated that mitochondrial proteins were over-represented in the liver from the two models of NASH (e.g., mouse fed a MCD diet or CD-HFD). This is in line with other studies reporting that intra-mitochondrial *O*-GlcNAcylation modulates OXPHOS function and ROS release in the heart [37], mitochondrial morphology, function, and mass [38]. Indeed, our findings showed that overexpression of OGT in hepatocytes inhibited mitochondrial function, while silencing OGT increased mitochondrial function, and that this was associated to a reduction and increase of intracellular fatty acid content. These effects are in agreement with the fact that the impaired hepatic mitochondrial function has been shown to be significantly associated to the development and progression of NAFLD [39,40]. To note, the beneficial effects of hepatic knockdown of OGT were not associated with a reduction in endoplasmic reticulum stress. Although this may seem paradoxical, it was proposed that OGT acts in flexible regions of target proteins (such as loops and termini) that can bind to its active site in an extended conformation to expose the amide backbone (PMID: 21240259). Therefore, under normal physiological conditions, only specific proteins would be modified, owing to the limited number of flexible elements in most mature proteins. However, during cellular stress, the availability of these elements increases given the accumulation of unfolded proteins in the cytoplasm and within cellular compartments, conditions under which *O*-GlcNAcylation is also dramatically elevated. Thus, our results showing a pronounced increase in the levels of endoplasmic reticulum stress-related proteins that are not downregulated by OGT silencing supports this hypothesis and pinpoints that endoplasmic reticulum stress might be an upstream mechanism of elevated *O*-GlcNAcylation.

In summary, our findings show that: a) *O*-GlcNAcylation is increased in the liver of mouse models and of patients with NASH, who also show a positive correlation between *O*-GlcNAcylation with fibrosis and NAS score; b) OGT inhibition in hepatocytes ameliorates diet-induced fibrosis; and c) this liver protection is mediated by an enhancement in mitochondrial activity. Overall, our results point towards an important role of *O*-GlcNAcylation in the pathogenesis of NAFLD progression.

AUTHOR CONTRIBUTIONS

M.J. G-R, V.H., T.P., and R.N.: concept and design and writing of article. A.R., M.F.F., E.N., N.L., M. V-R., A.S., M.D.P. C-V, C.A., D.G., M.F., S.B., C.D., M.L. M-C, O.M., J.M.M, M.S., V.P., J.C., G.F., P.I.: experiments and procedures and writing of article.

DECLARATION OF COMPETING INTEREST

The authors declare no conflict of interest

DATA AVAILABILITY

Data will be made available on request.

ACKNOWLEDGEMENTS

This work was supported by grants from: FEDER/Ministerio de Ciencia, Innovación y Universidades-Agencia Estatal de Investigación (MLM-C: PID2020-117116RB-I00; CD: BFU2017-87721; ML: RTI2018—101840-B-I00; RN: PID2021-126096NB-I00 and RED2018-102379-T); Xunta de Galicia (RN: 2021-CP085 and 2020-PG0157); Fundación BBVA (to RN); Subprograma Retos Colaboración RTC2019-007125-1 (to MLM-C); Proyectos Investigación en Salud DTS20/00138 (to MLM-C); Proyectos Investigación en Salud (MLMC: DTS20/00138); Fundación Atresmedia (to ML and RN), Fundación La Caixa (to ML and RN); la Caixa Foundation Program HR17-00601 (to MLM-C); Gilead Sciences International Research Scholars Program in Liver Disease (to MVR); and the European Foundation for the Study of Diabetes (to RN and GS). This research also received funding from the European Community's H2020 Framework Programme (ERC Synergy Grant-2019-WATCH-810331, to RN, VP and MS). The Centro de Investigación Biomédica en Red (CIBER) de Fisiopatología de la Obesidad y Nutrición (CIBERobn) and the Centro de Investigación Biomédica en Red (CIBER) de Enfermedades Hepáticas y Digestivas (CIBERehd) are initiatives of the Instituto de Salud Carlos III (ISCIII) of Spain, which is supported by FEDER funds. We thank MINECO for the Severo Ochoa Excellence Accreditation bioGUNE (SEV-2016-0644) to CIC.

APPENDIX A. SUPPLEMENTARY DATA

Supplementary data to this article can be found online at https://doi.org/10.1016/j.molmet.2023.101776.

REFERENCES

[1] Younossi ZM, Koenig AB, Abdelatif D, Fazel Y, Henry L, Wymer M. Global epidemiology of nonalcoholic fatty liver disease-meta-analytic assessment of prevalence, incidence, and outcomes. Hepatology 2016;64(1):73—84.

[2] Gastaldelli A, Cusi K. From NASH to diabetes and from diabetes to NASH: mechanisms and treatment options. JHEP Rep 2019;1(4):312—28.

[3] Harrison SA, Gawrieh S, Roberts K, Lisanti CJ, Schwope RB, Cebe KM, et al. Prospective evaluation of the prevalence of non-alcoholic fatty liver disease and steatohepatitis in a large middle-aged US cohort. J Hepatol 2021;75(2):284—91.

[4] Chitturi S, Abeygunasekera S, Farrell GC, Holmes-Walker J, Hui JM, Fung C, et al. NASH and insulin resistance: insulin hypersecretion and specific association with the insulin resistance syndrome. Hepatology 2002;35(2):373—9.

[5] Targher G, Corey KE, Byrne CD, Roden M. The complex link between NAFLD and type 2 diabetes mellitus — mechanisms and treatments. Nat Rev Gastroenterol Hepatol 2021;18(9):599—612.

[6] Yang X, Ongusaha PP, Miles PD, Havstad JC, Zhang F, So WV, et al. Phosphoinositide signalling links *O*-GlcNAc transferase to insulin resistance. Nature 2008;451(7181):964—9.

[7] Lagerlof O, Slocomb JE, Hong I, Aponte Y, Blackshaw S, Hart GW, et al. The nutrient sensor OGT in PVN neurons regulates feeding. Science 2016;351(6279):1293—6.

[8] Banerjee PS, Lagerlof O, Hart GW. Roles of *O*-GlcNAc in chronic diseases of aging. Mol Aspect Med 2016;51:1—15.

[9] Issad T, Lefebvre T. Editorial: *O*-GlcNAcylation: expanding the frontiers. Front Endocrinol 2019;10:867.

[10] Petersen MC, Vatner DF, Shulman GI. Regulation of hepatic glucose metabolism in health and disease. Nat Rev Endocrinol 2017;13(10):572—87.

[11] Yang X, Qian K. Protein *O*-GlcNAcylation: emerging mechanisms and functions. Nat Rev Mol Cell Biol 2017;18(7):452—65.

[12] Whelan SA, Dias WB, Thiruneelakantapillai L, Lane MD, Hart GW. Regulation of insulin receptor substrate 1 (IRS-1)/AKT kinase-mediated insulin signaling by O-linked beta-N-acetylglucosamine in 3T3-L1 adipocytes. J Biol Chem 2010;285(8):5204—11.

[13] Martinez MR, Dias TB, Natov PS, Zachara NE. Stress-induced *O*-GlcNAcylation: an adaptive process of injured cells. Biochem Soc Trans 2017;45(1):237—49.

[14] Fardini Y, Masson E, Boudah O, Ben Jouira R, Cosson C, Pierre-Eugene C, et al. *O*-GlcNAcylation of FoxO1 in pancreatic beta cells promotes Akt inhibition through an IGFBP1-mediated autocrine mechanism. FASEB J 2014;28(2):1010—21.

[15] Gorg B, Karababa A, Schutz E, Paluschinski M, Schrimpf A, Shafigullina A, et al. O-GlcNAcylation-dependent upregulation of HO1 triggers ammonia-induced oxidative stress and senescence in hepatic encephalopathy. J Hepatol 2019;71(5):930—41.

[16] Duan F, Wu H, Jia D, Wu W, Ren S, Wang L, et al. O-GlcNAcylation of RACK1 promotes hepatocellular carcinogenesis. J Hepatol 2018;68(6):1191—202.

[17] Xu W, Zhang X, Wu JL, Fu L, Liu K, Liu D, et al. O-GlcNAc transferase promotes fatty liver-associated liver cancer through inducing palmitic acid and activating endoplasmic reticulum stress. J Hepatol 2017;67(2):310—20.

[18] Santos-Laso A, Perugorria MJ, Banales JM, O-GlcNAcylation. Undesired tripmate but an opportunity for treatment in NAFLD-HCC. J Hepatol 2017;67(2):218—20.

[19] Gallage S, Avila JEB, Ramadori P, Focaccia E, Rahbari M, Ali A, et al. A researcher's guide to preclinical mouse NASH models. Nat Metab 2022;4(12):1632—49.

[20] Kleiner DE, Brunt EM, Van Natta M, Behling C, Contos MJ, Cummings OW, et al. Design and validation of a histological scoring system for nonalcoholic fatty liver disease. Hepatology 2005;41(6):1313—21.

[21] Covelo-Molares H, Souto Y, Fidalgo M, Guallar D. A simple, rapid, and cost-effective method for loss-of-function assays in pluripotent cells. Methods Mol Biol 2022;2520:199—213.

[22] Bernardo-Seisdedos G, Bilbao J, Fernandez-Ramos D, Lopitz-Otsoa F, Gutierrez de Juan V, Bizkarguenaga M, et al. Metabolic landscape of the mouse liver by quantitative (31) P nuclear magnetic resonance analysis of the phosphorome. Hepatology 2021;74(1):148—63.

[23] Zhang B, Li MD, Yin R, Liu Y, Yang Y, Mitchell-Richards KA, et al. O-GlcNAc transferase suppresses necroptosis and liver fibrosis. JCI Insight 2019;4(21).

[24] Sahai A, Pan X, Paul R, Malladi P, Kohli R, Whitington PF. Roles of phosphatidylinositol 3-kinase and osteopontin in steatosis and aminotransferase release by hepatocytes treated with methionine-choline-deficient medium. Am J Physiol Gastrointest Liver Physiol 2006;291(1):G55—62.

[25] Nossen JO, Rustan AC, Gloppestad SH, Malbakken S, Drevon CA. Eicosapentaenoic acid inhibits synthesis and secretion of triacylglycerols by cultured rat hepatocytes. Biochim Biophys Acta 1986;879(1):56—65.

[26] Ortiz-Meoz RF, Jiang J, Lazarus MB, Orman M, Janetzko J, Fan C, et al. A small molecule that inhibits OGT activity in cells. ACS Chem Biol 2015;10(6):1392—7.

[27] Horsch M, Hoesch L, Vasella A, Rast DM. N-acetylglucosaminono-1,5-lactone oxime and the corresponding (phenylcarbamoyl)oxime. Novel and potent inhibitors of beta-N-acetylglucosaminidase. Eur J Biochem 1991;197(3):815—8.

[28] Serra D, Mera P, Malandrino MI, Mir JF, Herrero L. Mitochondrial fatty acid oxidation in obesity. Antioxidants Redox Signal 2013;19(3):269—84.

[29] Liu R, Gou D, Xiang J, Pan X, Gao Q, Zhou P, et al. O-GlcNAc modified-TIP60/KAT5 is required for PCK1 deficiency-induced HCC metastasis. Oncogene 2021;40(50):6707—19.

[30] Chen Y, Bei J, Liu M, Huang J, Xie L, Huang W, et al. Sublethal heat stress-induced O-GlcNAcylation coordinates the Warburg effect to promote hepatocellular carcinoma recurrence and metastasis after thermal ablation. Cancer Lett 2021;518:23—34.

[31] Chu Y, Jiang M, Wu N, Xu B, Li W, Liu H, et al. O-GlcNAcylation of SIX1 enhances its stability and promotes Hepatocellular Carcinoma Proliferation. Theranostics 2020;10(21):9830—42.

[32] Cao B, Duan M, Xing Y, Liu C, Yang F, Li Y, et al. O-GlcNAc transferase activates stem-like cell potential in hepatocarcinoma through O-GlcNAcylation of eukaryotic initiation factor 4E. J Cell Mol Med 2019;23(4):2384—98.

[33] Chen Y, Liu R, Chu Z, Le B, Zeng H, Zhang X, et al. High glucose stimulates proliferative capacity of liver cancer cells possibly via O-GlcNAcylation-dependent transcriptional regulation of GJC1. J Cell Physiol 2018;234(1):606—18.

[34] Nguyen L, Masouminia M, Mendoza A, Samadzadeh S, Tillman B, Morgan T, et al. Alcoholic hepatitis versus non-alcoholic steatohepatitis: levels of expression of some proteins involved in tumorigenesis. Exp Mol Pathol 2018;104(1):45—9.

[35] Ong Q, Han W, Yang X. O-GlcNAc as an integrator of signaling pathways. Front Endocrinol 2018;9:599.

[36] Shafi R, Iyer SP, Ellies LG, O'Donnell N, Marek KW, Chui D, et al. The O-GlcNAc transferase gene resides on the X chromosome and is essential for embryonic stem cell viability and mouse ontogeny. Proc Natl Acad Sci U S A 2000;97(11):5735—9.

[37] Dontaine J, Bouali A, Daussin F, Bultot L, Vertommen D, Martin M, et al. The intra-mitochondrial O-GlcNAcylation system rapidly modulates OXPHOS function and ROS release in the heart. Commun Biol 2022;5(1):349.

[38] Akinbiyi EO, Abramowitz LK, Bauer BL, Stoll MSK, Hoppel CL, Hsiao CP, et al. Blocked O-GlcNAc cycling alters mitochondrial morphology, function, and mass. Sci Rep 2021;11(1):22106.

[39] Ajaz S, McPhail MJ, Gnudi L, Trovato FM, Mujib S, Napoli S, et al. Mitochondrial dysfunction as a mechanistic biomarker in patients with non-alcoholic fatty liver disease (NAFLD). Mitochondrion 2021;57:119—30.

[40] Meex RCR, Blaak EE. Mitochondrial dysfunction is a key pathway that links saturated fat intake to the development and progression of NAFLD. Mol Nutr Food Res 2021;65(1):e1900942.

